Available online at www.sciencedirect.com
ScienceDirect
Journal of the European Ceramic Society 27 (2007) 2485–2494
www.elsevier.com/locate/jeurceramsoc

Fatigue crack growth law for ferroelectrics under cyclic electrical and combined electromechanical loading

Ilona Westram [a], Andreas Ricoeur [b,*], Andreas Emrich [b], Jürgen Rödel [a], Meinhard Kuna [b]

[a] *Institute of Materials Science, TU Darmstadt, Petersenstraße 23, 64287 Darmstadt, Germany*
[b] *Institute of Mechanics and Fluid Dynamics, TU Bergakademie Freiberg, Lampadiusstraße 4, 09596 Freiberg, Germany*

Received 22 May 2006; received in revised form 29 August 2006; accepted 10 September 2006
Available online 27 October 2006

Abstract

New data sets of crack propagation in lead-zirconate-titanate DCB specimens under cyclic electric loading combined with a constant mechanical load have been obtained. Both an increasing mechanical load as well as an increasing field amplitude resulted in an enhanced crack propagation rate. The experiment was modelled with a Finite Element Analysis that used special crack tip elements and assumed a finite permeability of the crack. The calculations revealed a dielectric crack closure effect, explaining the experimentally observed threshold of fatigue crack growth for the electric load. Fracture quantities suitable for cyclic loading by electric fields above the coercive field were discussed and a Mode-IV intensity factor considered as appropriate. The resulting correlations were applied to the experimental results and a power law relationship for the crack growth rate versus the range of the Mode-IV intensity factor was found.

Keywords: Cracking; PZT; Mechanical properties; Piezoelectric properties; Fatigue

1. Introduction

Nowadays ferroelectric ceramics are used in a wide variety of applications such as fuel injection valves, transducers or memory devices (FeRAMs). Depending on the application, the direct or indirect piezoeffect is exploited, therefore the material is subjected to cyclic or static mechanical, electrical or combined electromechanical loading. Under these loading conditions, micro- or macrocracking can occur in the material and eventually lead to failure of the device.[1] In this paper, the phenomenon of macrocrack propagation in a ferroelectric material under purely cyclic electric fields or cyclic electric fields in combination with a static mechanical load is investigated.

Compared to fatigue crack-growth in structural ceramics under cyclic mechanical loading, the failure mechanism in electrically cycled ferroelectrics results from inelastic deformations in the fracture process zone causing stresses at the crack tip. These stresses induce a stress intensity factor which reaches the fracture toughness periodically. Thus, crack growth is not subcritical on the microstructural level. The spontaneous strain and changes of polarization are caused by domain wall motion which is due to ferroelectric/ferroelastic domain switching. Mechanical cycling of ferroelectrics involves both mechanisms of classical subcritical crack growth (e.g. stress corrosion) and effects due to domain switching. However, interpreting experimental studies by different authors,[2–4] classical crack propagation mechanisms seem to dominate there. Therefore, our investigations focus on electric cycling.

First works on this topic were performed in the 1990s[5–9] with cracks emanating from Vickers indents. In later works, through-thickness cracks were used.[10–12] Cyclic electric fields of different field strengths were applied and crack growth was observed mainly in the direction perpendicular to the electric field. It was found that a certain field level is needed to be surpassed in order for a crack to propagate. This level differed slightly from experiment to experiment but usually lay above the coercive field strength of the respective material. In one case, crack propagation was also observed for lower fields.[9] Generally, the crack growth rate was observed to increase with increasing applied field amplitude but to decrease with increasing cycle numbers.

Crack propagation under cyclic mechanical loading in PZT has only been studied by few groups.[2,13] Jiang and Sun applied a constant electrical field in addition to the cyclic mechanical

* Corresponding author. Tel.: +49 3731 392699; fax: +49 3731 393455.
E-mail address: Andreas.Ricoeur@imfd.tu-freiberg.de (A. Ricoeur).

0955-2219/$ – see front matter © 2006 Elsevier Ltd. All rights reserved.
doi:10.1016/j.jeurceramsoc.2006.09.010

loading and reported a power-law relationship between the crack growth rate and the amplitude of the mechanical energy release rate. Salz et al.[2] used static and cyclic mechanical loads and also observed a power-law relationship between the cyclic load amplitude and the crack growth rate. The approach of describing the crack growth rate in piezoelectric materials with a Paris law relationship is based on results from theoretical modelling.[14]

To date, no experiments have been performed with the combination of a static mechanical and a cyclic electrical load. For our study, a *D*ouble *C*antilever *B*eam (DCB) specimen is used which can be loaded by an alternating electric field perpendicular to the plane of crack propagation and a mechanical force producing a Mode-I crack opening. In contrast to cracks initialized by Vickers indentations, a through-thickness crack in a fracture mechanics specimen provides reproducible loading conditions and predictable crack paths. Experiments on such a specimen are necessary for an appropriate evaluation of the data within a fracture mechanics framework and for the derivation of a transferable crack growth law.

A numerical analysis of the coupled electromechanical field problem is performed accounting for a limited electrical permeability of the crack. It reveals the physical nature of a crack closure effect, which is responsible for cracks not growing under pure electrical loads below the coercive field. In order to have an objective, geometrically-independent characterization of the crack tip loading, a fracture quantity is subsequently calculated. Since domain switching is not restricted to the crack tip zone (large scale switching), and since the material exhibits a pronounced hysteretic behavior during a loading cycle, the application of one of the classical fracture mechanical quantities is not obvious.

In the experiments, different combinations of mechanical and electrical loads were used and the crack propagation rates measured in each case. Together with the numerical calculations a general fatigue crack growth law for a commercial lead-zirconate-titanate composition is derived having the same structure as the classical Paris Law. Until now, only one similar fracture mechanical evaluation has been done by Fang et al.,[12] however based on simplified analytical calculations.

2. Experiment

2.1. Material and specimen preparation

Specimens for the experiments were provided by PI Ceramics (Lederhose, Germany) in the form of double cantilever beams, 40 mm × 5 mm × 1.5 mm in dimension. The material PIC151 was used which is a lead-zirconate-titanate composition near the *m*orphotropic *p*hase *b*oundary (MPB): $Pb_{0.99}(Zr_{0.45}Ti_{0.47}(Ni_{0.33}Sb_{0.67})_{0.08})O_3$. It is a commercially used, soft ferroelectric material. All specimens were first polished down to a 1 μm finish on one of their 40 mm × 5 mm faces. Next they were electroded with a conducting silver paste ("Leitsilber 200", Hans Wolbring GmbH, Germany) on their 40 mm × 1.5 mm faces. Next they were poled in a bath of silicon oil (AK35, Wacker Chemie GmbH, Germany, dielectric strength > 12 kV/mm) for 20 min at room temperature and a field strength of $2E_C$, E_C being the coercive field strength of the material, which lies around 1 MV/m.

One part of the specimens was cycled purely electrically without an additional mechanical load. A diamond-wire saw (Wells 2040) was used to provide them with a 1 mm-long and 0.2 mm-wide through-thickness notch with a radius of 0.1 mm at the ground. A sketch of the specimen geometry is depicted in Fig. 1a.

The specimens tested under combined loading conditions were provided with a hole of 2.5 mm in diameter and an 8 mm-long and 0.2 mm-wide through-thickness notch (see Fig. 1b for a sketch). Next they were one by one subjected to one half-cycle of an electric field of $1.5E_C$ opposite to the poling direction. This resulted in a crack "popping" into the specimen from the notch, the crack faces being perpendicular to the electric field. The length of this crack was 0.5 mm with a variation from specimen to specimen of ±50 μm. Then the specimens were set aside for a period greater than 24 h in order for any relaxation processes and backswitching to occur before the crack propagation experiments were conducted.

2.2. Experimental set up and measurements

One specimen at a time was placed into a container filled with silicon oil (see Fig. 2a). This provided protection against electrical breakdown. In addition, a thin glass plate covered the specimen. The container with the specimen was then placed underneath an optical microscope (Leica DM LM) onto an X-Y-stage. Crack lengths were measured optically with a resolution of 5 μm. For the generation of the sinusoidal electric field, a function generator (TGA1240, TT*i*, England) in connection to a HV power supply (HCB 500 M—10,000, F.u.G. Elektronik GmbH, Germany) was used. The sample was contacted at its unnotched end by means of two metal springs.

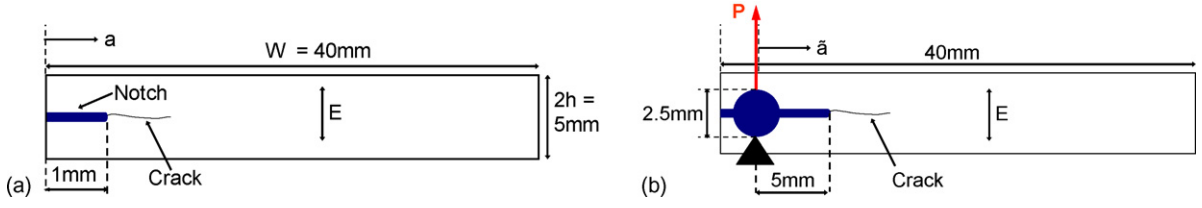

Fig. 1. Specimen geometries for (a) cyclic electric loading and (b) combined electromechanical loading with a mechanical preload and a cyclic electric field. The specimen thickness is $b = 1.5$ mm.

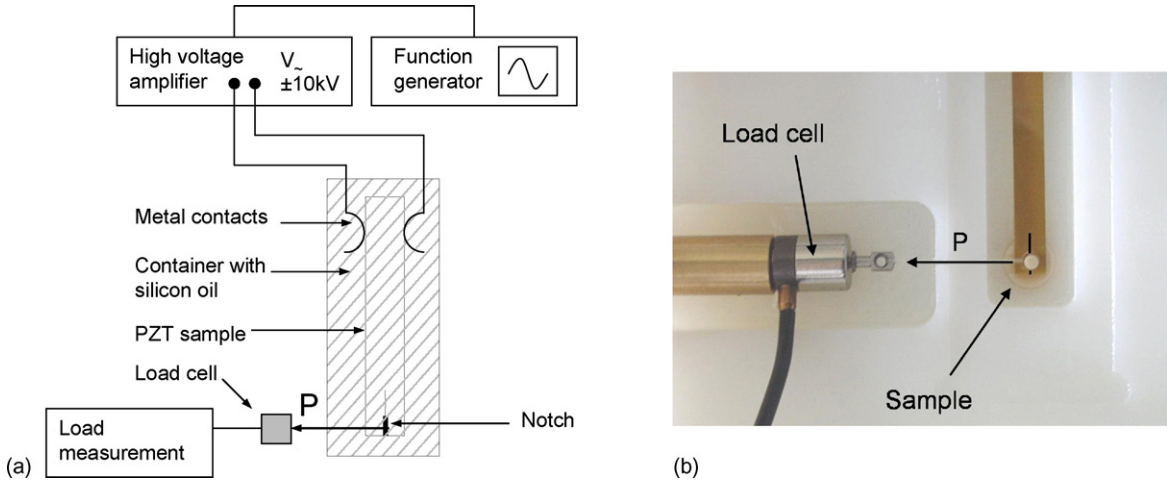

Fig. 2. (a) Schematic of experimental setup. (b) Picture of specimen for cycling under a constant mechanical and cyclic electrical load.

2.2.1. Electrical cycling

A total of 14 specimens was used for the electrical cycling with different field amplitudes: one specimen each was cycled at 0.9, 1.1 and $1.8E_C$, two specimens each were cycled at 1.2, 1.7 and $1.9E_C$ and three specimens each were cycled at 1.3 and $1.5E_C$.

The mean values of the electric fields were zero, thus an amplitude ratio $R = E_{min}/E_{max} = -1$ prevails. A minimum of 60 sinusoidal cycles with a frequency of 1 Hz was applied to each specimen. The crack length was measured every five cycles during a short (~5–10 s) break in cycling. It could not be measured in situ since the specimen moved during cycling due to its transverse contraction.

2.2.2. Mechanical preload + electrical cycling

The combined loading tests consisted of a static mechanical load causing a constant Mode-I stress intensity factor ranging from 0.1 to 0.5 MPa $\sqrt{m}$ and a cyclic electrical load ranging from 0.3 to $1.7E_C$. The intrinsic fracture toughness of the material is about 0.77 MPa $\sqrt{m}$.[15] A total of 29 different combinations of mechanical and electrical load were used which are displayed in Fig. 3. One specimen was used per combination.

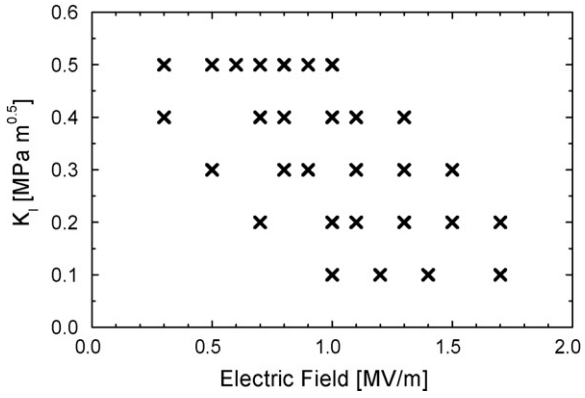

Fig. 3. Combinations of static mechanical load – in terms of stress intensity factor K_I – and cyclic electric load – in terms of the amplitude – used in the experiments. For each load combination a new specimen was used.

The mechanical load was applied by fixing one arm of the cantilever with a ceramic pin and connecting the other arm to a 30 N load cell using a nylon thread. This is also shown in Fig. 2b. The load was adjusted through a threaded connection and a metal spring. To keep the stress intensity factor constant during electrical cycling, the load was adjusted with increasing crack length. The respective values were calculated with Kanninen's formula:[16]

$$P = K_I \frac{b\,h^{3/2}}{2\sqrt{3}\,\tilde{a}} \frac{1}{(1 + 0.64\,h/\tilde{a})} \quad (1)$$

where P is the applied force, K_I the Mode-I stress intensity factor, $\tilde{a}$ the distance between the point of load application and the crack tip, $2h$ the specimen height and b is the specimen thickness (see Fig. 1). This formula is a very good approximation, if the crack tip does not approach the end of the specimen by less than 2 h and if $a/h > 2$. Due to the short crack lengths investigated and the sufficiently long notch, this was always guaranteed.

2.3. Results

In the case of pure electrical cycling, no crack growth occurred for field amplitudes below $1.1E_C$. It was observed that the primary crack propagated with an approximately constant crack growth rate during the first 10–30 cycles. The duration of this so-called "steady-state" varied from specimen to specimen. In the next stage, one or more secondary cracks formed which either propagated sequentially or simultaneously. Generally, a decrease in crack growth rate was observed with increasing cycle number.

In the case of combined loading, the crack path was observed to be unstable for combinations of large mechanical and electrical loads. In that case, the crack gradually kinked and the specimen broke before 60 electric field cycles were reached. Representative results of crack length versus cycle number for either one electrical load and different stress intensity factors or one stress intensity factor and different electrical loads are displayed in Figs. 4 and 5. Both an increasing K_I as well as an

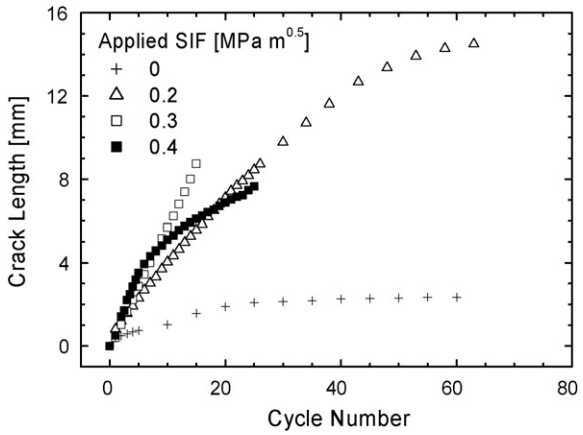

Fig. 4. Crack length vs. cycle number for applied stress intensity factors between 0 – purely electrical loading – and 0.4 MPa $\sqrt{m}$. The electrical loading amplitude was $1.3E_C$. For $K_I = 0.3$ and 0.4 MPa $\sqrt{m}$ the specimens broke due to unstable crack paths before 60 cycles were reached.

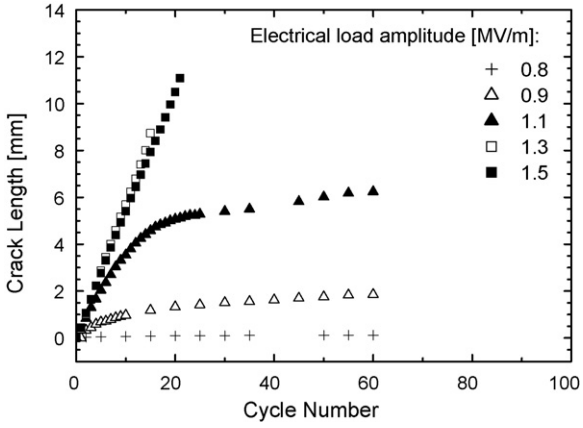

Fig. 5. Crack length displayed vs. cycle number for an applied stress intensity factor of 0.3 MPa $\sqrt{m}$ and different electric loading amplitudes as denoted in the figure. For $E = 1.3$ and $1.5E_C$, the specimens fractured before 60 cycles were reached due to unstable crack paths.

increasing field amplitude resulted in an increased crack growth rate.

After both the electrical loading and the combined loading experiments, the fracture surfaces were examined in a scanning electron microscope and compared to fracture surfaces resulting from static mechanical loading. Exemplary pictures are provided in Fig. 6. In the electrical and electromechanical loading cases, mainly transgranular fracture occurred, while under mechanical loading, a mixture of trans- and intergranular fracture was observed. This might indicate that the fracture mechanism under electrical loading is dominant to the fracture mechanism under mechanical loading.

3. Fracture mechanical evaluation of the experimental data

The measurements in the previous section supply crack growth rates for specific loading and poling configurations and are valid for the specific specimen geometry. For the sake of a unique and objective quantification of the crack tip loading within the range of a fracture mechanics concept, crack growth rates have to be presented as functions of fracture mechanics quantities, e.g. K-factors, the energy release rate or the J-integral. For the specimen and loading conditions of the experiment as well as for structures in arbitrary applications, the fracture quantities are calculated using the Finite Element Method.

3.1. Discussion of fracture quantities

If domain switching is restricted to a small zone close to the crack tip (small-scale-switching), concepts of Linear Elastic Fracture Mechanics can be generalized for piezoelectric fracture mechanics. In this case, the K-concept is applicable and the loading of the crack tip can be expressed by a Mode-IV intensity factor.[17] For a DCB specimen with the height $2h$ and the applied electric field E_2^∞ the following formula is commonly used.[12]

$$K_E = \lim_{r\to 0}\left(\sqrt{2\pi r}E_2(\theta = 0)\right) = E_2^\infty\sqrt{2h} \tag{2}$$

E_2 is the electric field strength in the x_2-direction, (r,θ) is a crack tip polar coordinate system (see Fig. 8). However, since fatigue crack growth at low electric cycling frequencies without mechanical loading is only observed for electric field intensities above the coercive field, the assumption of small-scale-switching is not applicable. Considering Elastic-Plastic Fracture Mechanics, the J-integral can be calculated in the case of large-scale inelastic material behavior. However, the

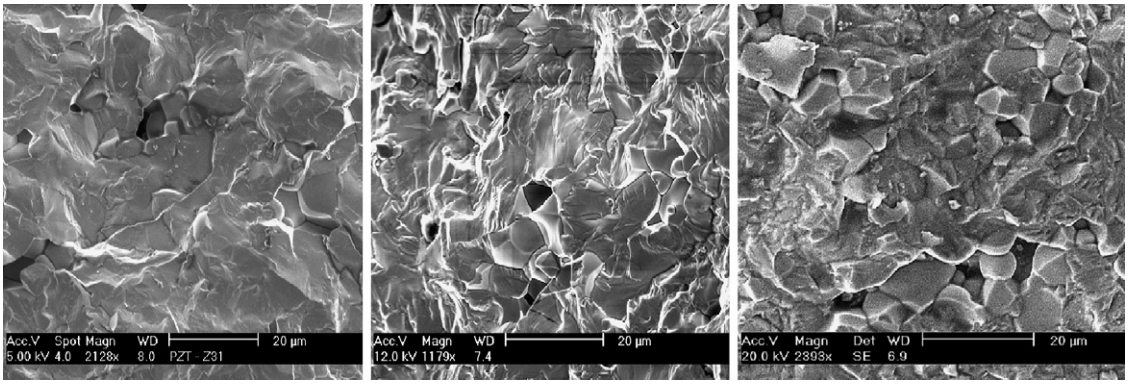

Fig. 6. Fracture surfaces after electrical loading (left), electromechanical loading (center), mechanical loading (right).

J-integral for cyclic loading is not path-independent for materials showing an inelastic dissipative behavior. Its application therefore is not the appropriate means for a unique characterization of the crack tip loading.

In contrast to plasticity, where an increasing load leads to a continuous enhancement of plastic strain, in ferroelectrics a "lock-in" is observed, i.e. the microstructural evolution is saturated reaching a specific loading level. Beyond this threshold loading and unloading follow the same trajectory and the material behavior is described by linear constitutive equations of piezoelectricity, even being a good representation somewhat below the saturation point. Thus, during electric cycling with amplitudes above the coercive field, the specimen is not subject to material non-linearities during the whole cycle. In Fig. 7 a load cycle $E(t)$ is shown schematically starting with an electric field pointing into the poling direction. The coercive field E_C is indicated by the horizontal dashed lines. If the electric load amplitude is within the hatched area (1), small-scale-switching can be assumed. The cross-hatched areas (2) represent field intensities at which the material sufficiently remote from the crack is always homogeneously poled in the loading direction and may be described linearly. The applicability of piezoelectric constitutive equations is justified within the one half of the loading cycle in which the electric field is aligned with the poling direction. Physical non-linearities due to domain switching dominate the material behavior during the small part of the cycle indicated by a bold line. It was observed experimentally[18] that this is the point of the cycle, where crack growth sets in. Westram et al. therefore believe that large-scale switching provides the driving force for crack initiation. The mechanism is explained in Ref.[18] in more detail. However, the crack growth rate was found to depend on the field amplitude, i.e. on how much larger than E_C the maximum field is. To describe this observation phenomenologically, the K-concept of Linear Elastic Fracture Mechanics can be applied to characterize the loading conditions at the crack tip during the greatest part of the cycle. A Mode-IV intensity factor K_{IV} is introduced characterizing the asymptotic behavior of the electric displacement D_2 in front of the crack tip. Its definition is similar to K_E in Eq. (2) replacing E_2^∞ by D_2^∞. Due to the repeated repolarization, the remote electric field is directed parallel to the poling direction almost during the whole loading cycle, leading to an almost permanent positive K_{IV} (see Fig. 7). Therefore, the range ΔK_{IV} approximately equals K_{IV}^{max}. During the process of massive domain reorientation the field intensity factor is not defined since piezoelectric properties are lost. K_{IV}^{max} meets the requirements of a fracture mechanical quantity giving a unique and transferable characterization of the loading situation.

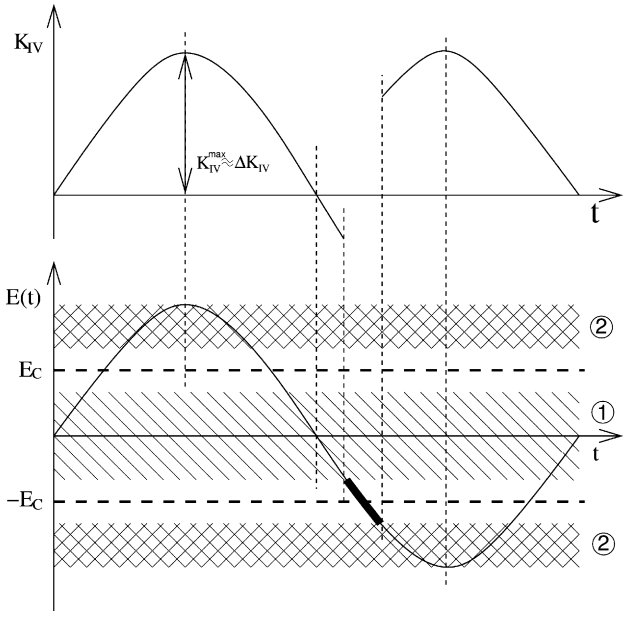

Fig. 7. One electric loading cycle with intervals of linear and non-linear material behavior (bottom) and schematic of the course of the electric displacement intensity factor (top).

3.2. Finite element calculations

To calculate field intensity factors and other fracture mechanical quantities for cracks in piezoelectrics, several numerical techniques based on the Finite Element Method have been developed.[19–21] Derived by rudimentary analytical calculations, Eq. (2) is considered not to be sufficiently accurate. Particularly concerning short cracks the crack length has a non-negligible influence on K_{IV}. Moreover, the electric boundary conditions on the crack faces should be chosen more carefully thus being closer to reality. The specimen is assumed to be homogeneously poled, which is obviously simplifying the nature of the problem. More sophisticated calculations could account for the inhomogeneous state of polarization in the vicinity of the crack. Anyhow, to determine K_{IV}, the asymptotic crack tip solution has to be known. For an inhomogeneous polarization, those solutions are rare in the literature[22,23] and treat special cases which are not relevant for our problem. The calculation of intensity factors neglecting the polarization inhomogeneity is well established in the evaluation of fracture experiments in piezoelectrics under constant loading conditions.[21,22,24,25] On the other hand, the electromechanical energy release rate can be determined, e.g. applying the Modified Crack Closure Integral.[19,21] The comparison of calculations for a crack in a material being on the one hand homogeneously poled and on the other hand showing the typical near-crack domain pattern exhibited very little influence on the energy release rate. However, numerical calculations have shown that a criterion for electrical-load-induced fracture cannot be based on either the electromechanical or the pure mechanical/electrical energy release rates, since none of these quantities correctly reflects the influence of the investigated loading regimes on the crack growth behavior.

Fig. 8 shows the Finite Element model of the specimen used for combined electromechanical loading. For pure electrical loading the model is identical except for the hole, which mildly influences the crack tip fields. Due to symmetry, only one half has to be considered. On the ligament, the nodal boundary conditions $u_2 = 0$, $\phi = 0$ are introduced, where u_2 is the displacement in the x_2-direction and ϕ is the electric potential. A generalized state of plane strain is assumed for the 2D model, i.e. $\partial u/\partial x_3 = 0$, $\partial \phi/\partial x_3 = 0$. The crack tip is indicated by the origin of the polar

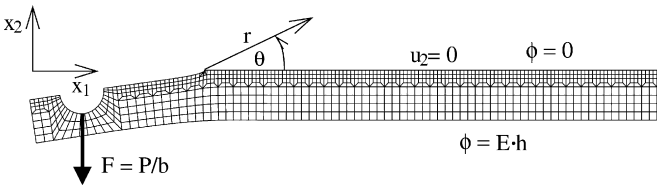

Fig. 8. Finite Element model of one half of the DCB specimen with boundary conditions and coordinate systems.

coordinate system (r,θ). Shifting the boundary conditions along x_1, various crack lengths can be realized with the same mesh. To calculate field intensity factors for different crack tip positions, this implies an evenly meshed layer around $x_2 = 0$. The loading is applied by a line force $F = P/b$ and the electrode potential $\phi = Eh$.

Both K_I and K_{IV} are calculated from displacements u_2 and electric potentials ϕ on the crack faces, determined by the FE analysis. Using special crack tip elements (CTE) which exhibit a $\sqrt{r}$-behavior, an accurate calculation of intensity factors is guaranteed in connection with the asymptotic piezoelectric crack tip solution.[19,24] It was shown that Eq. (1) is a good approximation for K_I. The Mode-I stress intensity factor hardly depends on electrical loads. The deviation from the numerical results is just a few percent. K_{IV} shows a pronounced dependence on both mechanical and electrical loads.

Following an idea of Hao and Shen,[26] the electric field inside the crack is taken into account imposing a charge density D_2^C on the crack faces calculated from a body cut

$$D_2^C(x_1, x_2 = 0) = -\kappa_C \frac{\phi^+(x_1) - \phi^-(x_1)}{u_2^+(x_1) - u_2^-(x_1)} \tag{3}$$

with the superscripts "+" and "−" standing for the positive and negative crack faces, respectively and κ_C being the dielectric constant of the slit. In contrast to impermeable ($D_2^C = 0$) or fully permeable ($\phi^+ = \phi^-$) crack models, the assumption of an electrically limited permeable crack is consistent from the electrostatic point of view. The short notch does not have to be modelled separately, since it proved not to influence the results in terms of intensity factors. The numerical realization of this "capacitor analogy" requires an iteration scheme. Several Finite Element calculations of the boundary value problem have to be performed, to make the fields on the crack faces finally satisfy Eq. (3).[28] Electrostatic tractions on the crack faces[29] are not taken into consideration, though they might have a certain influence on K_{IV} for small or vanishing mechanical loads. Also, the accumulation of free charges on the crack faces is neglected, since the specimen is embedded in silicon oil.

The crack slit is modelled as a dielectric with the permittivity of vacuum, i.e. $\kappa_C = \kappa_r\kappa_0 = 8.854 \times 10^{-12}$ C/(V m) ($\kappa_r = 1$). The silicon oil actually has a relative permittivity of 2.5, but measurements of Schneider et al.[27] found an increased permittivity of up to 40 in an indentation crack. They attributed this fact to possible crack bridging or a reduced potential difference due to charge compensation at the crack surfaces. Since the dielectric state is apparently not well-defined, the choice of vacuum permittivity seems as reasonable as any other.

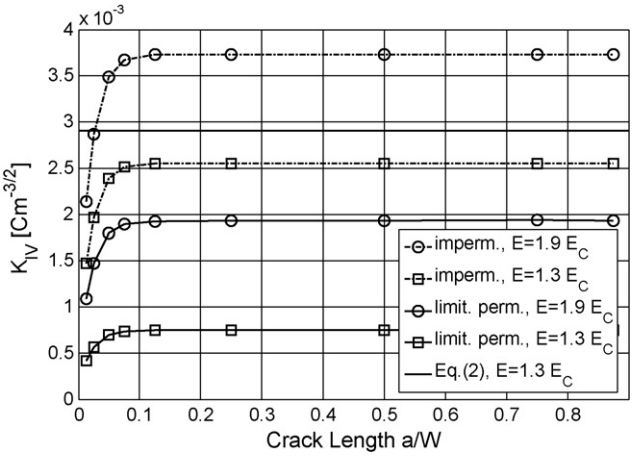

Fig. 9. Electric displacement intensity factor vs. normalized crack length for different crack face boundary conditions and electric loads.

Fig. 9 shows plots of the electric displacement intensity factor K_{IV} versus the crack length a related to the specimen length W (see Fig. 1). Different crack lengths between 0.5 and 35 mm indicated by the squares and circles have been investigated. Pure electric loading with field intensities of 1.3 and $1.9E_C$ is considered. Besides the limited permeable crack boundary condition Eq. (3), an impermeable crack with the boundary condition $D_2^C = 0$ has been investigated, assuming that the electric field totally circumvents the crack. This simplifying model overestimates the electric field concentration near the crack tip thus leading to higher values of K_{IV}. For $a/W > 0.1$ K_{IV} does not depend on the crack length, so the simple Eq. (2) could be applied in principle. The straight line at $K_{IV} \approx 2.9\,\mathrm{C\,m^{-3/2}}$ comes from Eq. (2) with $E_2^\infty = 1.3E_C$. K_{IV} in general can be calculated from a linear combination of K_I and K_E including the elastic, dielectric and piezoelectric constants of the material. Comparing this value to the numerical result for an impermeable crack boundary condition, a difference of approximately 12% is found. Anyway, $a/W < 0.1$ is the relevant range of parameters, because the experimental data are within this scope.

In Fig. 10 K_{IV} is plotted versus the normalized electric load E/E_C for different crack lengths and electrical crack face bound-

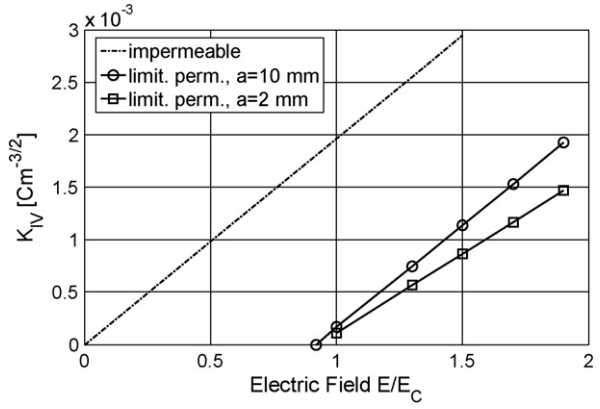

Fig. 10. Electric displacement intensity factor vs. electric load for different crack face boundary conditions and crack lengths. The impermeable line is valid for $a/W > 0.1$.

ary conditions. As in the previous figure, the specimen is not loaded mechanically. In all cases the electric displacement intensity factor does linearly depend on the electric far field. With impermeable crack faces the line goes through the origin of the coordinate system, i.e. $K_{IV} = 0$ for a vanishing load. The one exhibited in the graph holds for longer cracks $a/W > 0.1$. In the limited permeable case (solid line, circles) a parallel shift of the plot along the load-axis is observed. For shorter cracks (solid line, squares) the point of intersection with the abscissa $E^{clo} = 0.92E_C$ is unchanged, just the slope is different. Physically, E^{clo} is the threshold of an electrostatic crack closure effect. It essentially depends on the dielectric constants and represents an electric load which has to be exceeded to exhibit a crack driving mechanism in terms of a positive K_{IV}. Below E^{clo} the crack remains closed or in the absence of the implementation of a contact algorithm the crack faces may even overlap numerically and a negative intensity factor prevails. The latter case does not make sense from the physical point of view, so K_{IV} is always zero below E^{clo} and the electrical and mechanical fields are homogeneous not exhibiting any crack tip singularity. The threshold for crack growth being close to the coercive field is confirmed by the experiment. It should be kept in mind that this result is based on piezoelectric calculations which do not contain E_C as a parameter. Mathematically, a bifurcation is the reason for the crack closure effect. The Hao and Shen model always yields two solutions satisfying Eq. (3), one being excluded due to physical interpretations. For a pure electrical loading D_2^C is similar to D_2^∞ if $E_2^\infty < E^{clo}$. For a crack in an infinite domain D_2^C is exactly identical to D_2^∞. Thus, there is a homogeneous electric field within the body, the crack is closed and the electric potential is continuous. Beyond the threshold the solution path bifurcates yielding (i) the closed-crack solution $D_2^C = D_2^\infty$ and (ii) a second electrostatically consistent charge density $D_2^C = \text{const.}$ D_2^C in case (ii) does not depend on the loading, since both electric potential and mechanical displacement on the crack faces grow likewise with increasing D_2^∞. According to Eq. (3), the magnitude of D_2^C only depends on the dielectric constant of the crack κ_C. Solution (ii) cannot occur below the point of bifurcation, i.e. $D_2^C = D_2^\infty$, because the magnitude of crack face charges must not exceed that of the loading. Only the case (ii) goes along with a crack opening displacement and a crack tip singularity allowing for the interpretation of crack growth mechanisms at pure electrical loading.

In Figs. 11 and 12 for the combined load case K_{IV} is plotted versus the electric field intensity and the Mode-I stress intensity factor, respectively. Still, there is a linear dependence on the electric load. The mechanical load opens the crack thus decreasing the electrical permeability of the slit. Therefore, an increasing K_I enhances the electric displacement intensity factor asymptotically approaching the impermeable state. This circumstance leads to a stepwise rise of the crack growth rate as soon as even a small mechanical load is imposed (see Fig. 4). The relation between K_{IV} and K_I is non-linear. From Fig. 11 the thresholds for crack closure are obtained by extrapolation of the straight lines to the abscissa. Without a mechanical load E^{clo} is $0.9E_C$. The slight difference to E^{clo} from Fig. 10 is due to the Finite Element models which differ in the hole for the mechanical

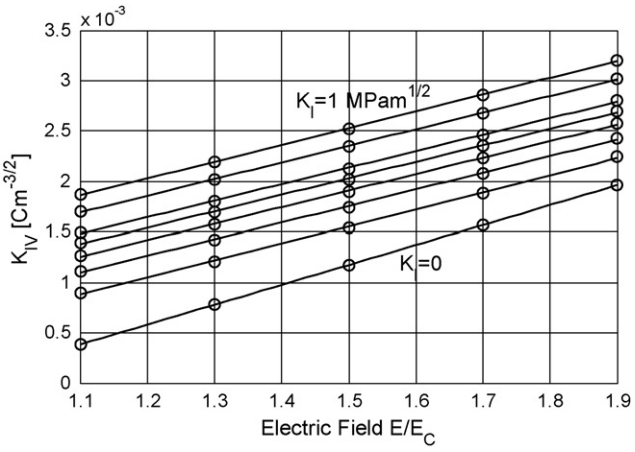

Fig. 11. Electric displacement intensity factor vs. electric load for different mechanical loads represented by the Mode-I stress intensity factor K_I.

force application. In the combined Mode-I/IV case a crack closure effect only exists for small mechanical loads, leading to a threshold value which may be significantly smaller than the coercive field. For the same values of K_I, Fig. 11 has been calculated with different crack lengths and the respective forces P leading to identical results. In Fig. 12, two crack lengths $a = 10$ and 30 mm are depicted, where $a = 0$ is selected at the leading edge of the specimen. The forces P applied to the Finite Element models for different crack lengths have been determined from Eq. (1). Thus, the close distances between squares and circles are a measurement for the accurateness of Eq. (1).

3.3. Correlations for the electric displacement intensity factor

To avoid the effort of performing numerical FE calculations for each experimental data set, closed-form equations are supplied for the calculation of K_{IV}. These correlations have been derived from Finite Element analyses interpolating discrete numerical values for several crack lengths and loads within the relevant range.

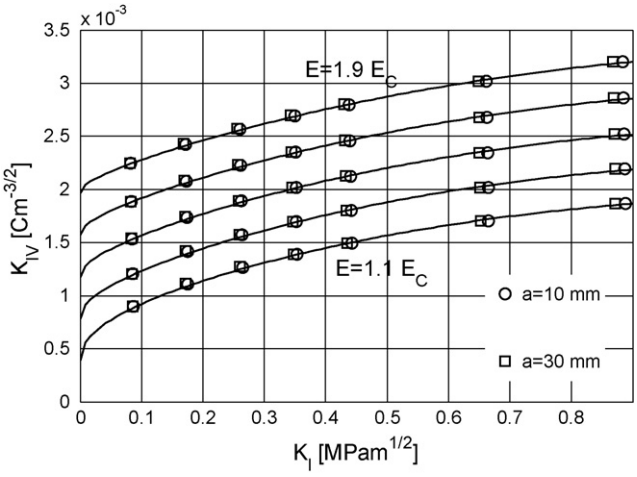

Fig. 12. Electric displacement intensity factor vs. Mode-I stress intensity factor for different electric loads and crack lengths.

From the model for pure electrical cycling the following equation is obtained:

$$K_{IV} = \left(1.85\sqrt{h}\kappa_{33}(E_2^{\infty} - E^{clo})\right) \times \left(1 - \frac{1}{(1 + 12(a/W))^6}\right); \quad E_2^{\infty} \geq E^{clo} \tag{4}$$

The dielectric constant of the solid κ_{33} was introduced to obtain coherent units and is 21.2×10^{-9} C/(V m) for PIC151. The relative crack length a/W has been introduced in Fig. 9 and $2h = 5$ mm is the specimen height. The threshold E^{clo} has been calculated to be 0.92 E_C and is used for the fracture mechanical evaluation of the experimental data. This value is sensitive to the choice of dielectric constants of the solid and towards the crack permeability used in the model. Moreover, crack closure effects due to domain switching could have an effect on E^{clo}. Therefore, under different circumstances it might differ from the observed threshold of electric field induced fatigue crack growth. In this case, it is appropriate to adopt the experimental value of E^{clo}, which produces a parallel shift of the solid lines along the abscissa in Fig. 10.

For the case of combined loading, the following equation is found:

$$K_{IV} = C_1(K_I)(E_2^{\infty} - E^{clo}) + C_2(K_I) \tag{5}$$

with the variables C_1 and C_2 depending on the Mode-I stress intensity factor which is calculated from Eq. (1):

$$C_1(K_I) = \left(\frac{m_1}{1 + m_2 K_I/(c_{33}\sqrt{h})} + m_3 + m_4\frac{K_I}{c_{33}\sqrt{h}}\right)\kappa_{33}\sqrt{h}$$

$$C_2(K_I) = \left(\frac{n_1}{1 + n_2 K_I/(c_{33}\sqrt{h})} + n_3 + n_4\frac{K_I}{c_{33}\sqrt{h}}\right)e_{33}\sqrt{h}$$

and the dimensionless constants m_1 to m_4 and n_1 to n_4 being

$$m_1 = 3.77 \times 10^{-1}, \quad n_1 = -1.5 \times 10^{-3}$$
$$m_2 = 138745, \quad n_2 = 40850$$
$$m_3 = 1.468, \quad n_3 = 1.5 \times 10^{-3}$$
$$m_4 = 492, \quad n_4 = 3.98$$

In Eq. (5), the crack closure threshold for purely electrical loading $E^{clo} = 0.9E_C$ is inserted. In contrast to the case of a single-mode electrical loading, governed by Eq. (4), the electric far field may now be smaller than E^{clo} but must not lead to negative intensity factors. The elastic and piezoelectric constants for PIC151 are $c_{33} = 10^5$ MPa and $e_{33} = 15.1$ C/m^2. Applying the Eqs. (4) and (5) the relative error within the relevant parameter range is below 3.5%. A much simpler correlation with the same accuracy is obtained, if the mechanical loading is restricted to $K_I \geq 0.2$ MPa $\sqrt{m}$:

$$K_{IV} = c_1\kappa_{33}\sqrt{h}(E_2^{\infty} - E^{clo}) + \left(c_2 + c_3\frac{K_I}{c_{33}\sqrt{h}}\right)e_{33}\sqrt{h} \tag{6}$$

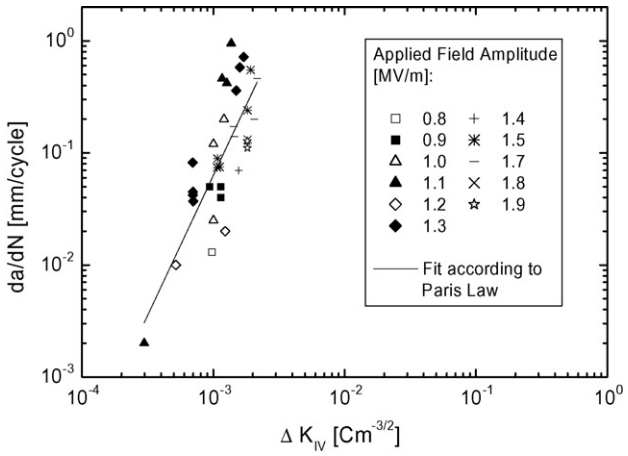

Fig. 13. Double-logarithmic plot of crack growth rate vs. ΔK_{IV} for different applied field amplitudes.

with only three empirical constants $c_1 = 1.556$; $c_2 = 8.26 \times 10^{-4}$; $c_3 = 6.76$.

3.4. Fatigue crack growth law

With the correlations (4) and (5) the experimental results were evaluated. Only the steady-state of crack propagation was considered and the crack growth rate was determined after 1 mm of crack propagation. For low mechanical and electrical loads, the crack growth rate was smaller than 0.001 mm/cycle and not considered for evaluation.

In Figs. 13 and 14, the crack growth rates are displayed versus ΔK_{IV} in double-logarithmic plots. In Fig. 13 different applied field amplitudes are marked by different symbols. The data can be described by a Paris-power-law relationship in the form of

$$\frac{da}{dN} = A \ \Delta K^m \tag{7}$$

with $A = 10^{6.33}$ and $m = 2.48$. The same data points are plotted in Fig. 14 with different symbols for different stress intensity factors. In the Paris Law there is no explicit dependence on

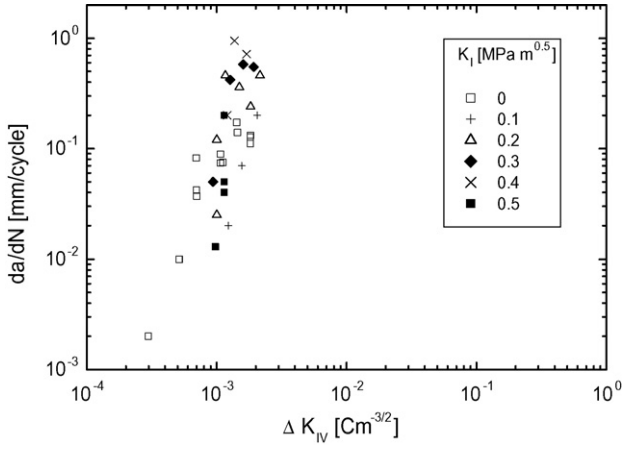

Fig. 14. Double-logarithmic plot of crack growth rate vs. ΔK_{IV} for different stress intensity factors between 0 – purely electrical loading – and 0.5 MPa $\sqrt{m}$.

K_I. The whole influence of the mechanical load is implicitly incorporated in its effect on K_{IV}.

4. Summary and conclusions

The paper provides investigations on the growth of fatigue cracks in ferroelectrics under low-cycle and high-amplitude loading conditions. Thus, crack growth rates are comparatively high. In contrast to other work available on this topic, the emphasis has been put on a careful and sophisticated numerical evaluation of the experimental data within the scope of a fracture mechanics concept. Crack growth rates are provided versus an electric displacement intensity factor, making the results independent of the specific geometry and loading conditions of the experiments.

Fatigue crack growth in PZT has been investigated experimentally. In contrast to previous work by different authors who applied cyclic electric fields, a constant mechanical load has been superimposed, effecting an additional Mode-I crack opening. For pure electrical loading, the amplitude has to exceed a threshold value which is slightly above the coercive field to evoke fatigue crack growth. Moreover, it was observed that the crack growth rate is enhanced by increasing the electrical load amplitude and decreases with increasing crack extension. Even small mechanical loads lead to a stepwise rise of the crack growth rate and reduce the threshold for an electrically driven crack to a value below the coercive field.

To provide conditions for a quantitative fracture mechanical evaluation of the experimental data, DCB specimens have been used for the experiments. In spite of some similarities between elastic–plastic and ferroelectric material behavior, there are fundamental differences. Thus, the *K*-concept of Linear Elastic Fracture Mechanics was found to be an appropriate means to describe crack tip loading, even if large-scale switching-conditions prevail. Thus, an electric displacement intensity factor K_{IV} was chosen as the appropriate fracture quantity for all load cases. The effect of the Mode-I crack opening is implicitly taken into account by the dependency of K_{IV} on K_I. A power law relating the crack growth rate and ΔK_{IV} was derived for combined electromechanical loading conditions.

The calculation of fracture quantities required a numerical solution of the piezoelectric boundary value problem. Based on linear constitutive equations, the Finite Element Method was applied to calculate fields within the specimen for the maximum values of an electric load cycle, where a microstructural domain evolution is either saturated ($E_{max} > E_C$) or does not exist ($E_{max} < E_C$). Adopting a capacitor analogy model, the crack faces were assumed to provide limited permeability from the dielectric point of view. A crack closure effect was revealed from the simulations, which explains the observed threshold value of electric load amplitudes being necessary to evoke fatigue crack growth. Future work could improve the accuracy of the numerical calculations accounting for an inhomogeneous poling state of the material, modelling electrostatic tractions on the crack faces and choosing the dielectric constant of the crack slit according to an appropriate model.

Acknowledgements

The authors would like to thank the German Research Corporation (DFG) for financial support under the contract numbers Ku 929/8 and Ro 954/17.

References

1. Furuta, A. and Uchino, K., Dynamic observation of crack propagation in piezoelectric multilayer actuators. *J. Am. Ceram. Soc.*, 1993, **76**, 1615–1617.
2. Salz, C. R. J., Hofmann, M., Westram, I. and Rödel, J., Cyclic fatigue crack growth in PZT under mechanical loading. *J. Am. Ceram. Soc.*, 2005, **88**, 1331–1333.
3. Zhu, T. and Yang, W., Fatigue crack growth in ferroelectrics driven by cyclic electric loading. *J. Mech. Phys. Solids*, 1999, **47**, 81–97.
4. Mao, G. Z. and Fang, D. N., Fatigue crack growth induced by domain switching under electromechanical load in ferroelectrics. *Theor. Appl. Fract. Mech.*, 2004, **41**, 115–123.
5. He, M.-Y., Suo, Z., McMeeking, R. M., Evans, A. G. and Lynch, C. S., The mechanics of some degradation mechanisms in ferroelectric ceramic actuators. *Proc. SPIE*, 1994, **2189**, 344–355.
6. Cao, H. and Evans, A. G., Electric-field-induced fatigue crack growth in piezoelectrics. *J. Am. Ceram. Soc.*, 1994, **77**, 1782–1786.
7. Lynch, C. S., Yang, W., Collier, L., Suo, Z. and McMeeking, R. M., Electric field induced cracking in ferroelectric ceramics. *Ferroelectrics*, 1995, **166**, 11–30.
8. Weitzing, H., Schneider, G. A., Steffens, J., Hammer, M. and Hoffmann, M. J., Cyclic fatigue due to electric loading in ferroelectric ceramics. *J. Eur. Ceram. Soc.*, 1999, **19**, 1333–1337.
9. Zhu, T., Fang, F. and Yang, W., Fatigue crack growth in ferroelectric ceramics below the coercive field. *J. Mater. Sci. Lett.*, 1999, **18**, 1025–1027.
10. Shieh, J., Fleck, N. A. and Huber, J. E., Observation of fatigue crack growth in ferroelectrics under electrical loading. *Proc. SPIE*, 2002, **4699**, 51–63.
11. Liu, B., Fang, D. N. and Hwang, K.-C., Electric-field-induced fatigue crack growth in ferroelectric ceramics. *Mater. Lett.*, 2002, **54**, 442–446.
12. Fang, D. N., Liu, B. and Sun, C. T., Fatigue crack growth in ferroelectric ceramics driven by alternating electric fields. *J. Am. Ceram. Soc.*, 2004, **87**, 840–846.
13. Jiang, L. Z. and Sun, C. T., Crack growth behavior in piezoceramics under cyclic loads. *Ferroelectrics*, 1999, **233**, 211–223.
14. Narita, F. and Shindo, Y., Mode 1 crack growth rate for yield strip model of a narrow piezoelectric ceramic body. *Theor. Appl. Fract. Mech.*, 2001, **36**, 73–85.
15. Kounga Njiwa, A. B., Fett, T., Lupascu, D. C. and Rödel, J., Crack-tip toughness of a soft lead zirconate titanate. *J. Am. Ceram. Soc.*, 2003, **86**, 1973–1975.
16. Kanninen, M. F., An augmented double cantilever beam model for studying crack propagation and arrest. *Int. J. Fract.*, 1973, **9**, 83–91.
17. Pak, Y. E., Linear electro-elastic fracture mechanics of piezoelectric materials. *Int. J. Fract.*, 1992, **54**, 79–100.
18. Westram, I., Oates, W. S., Lupascu, D. C., Rödel, J. and Lynch, C. S., Mechanism of electric fatigue crack growth in lead zirconate titanate. *Acta Mater.*, submitted for publication.
19. Kuna, M., Finite element analyses of crack problems in piezoelectric structures. *Comp. Mater. Sci.*, 1998, **13**, 67–80.
20. Abendroth, M., Groh, U., Kuna, M. and Ricoeur, A., Finite element-computation of the electromechanical *J*-Integral for 2-D and 3-D crack analysis. *Int. J. Fract.*, 2002, **114**, 359–378.
21. Kuna, M. and Ricoeur, A., Theoretical investigation of fracture behaviour in ferroelectric ceramics. *Fract. Mech. Ceram.*, 2002, **13**, 63–82.
22. Kemmer, G., Berechnung von elektromechanischen Intensitätsparametern bei Rissen in Piezokeramiken. *VDI Fortschritt-Berichte*, 2000, **261**, 20–23.
23. Chen, T.-H., Chue, C.-H. and Lee, H.-T., Stress singularities near the apex of a cylindrically polarized piezoelectric wedge. *Arch. Appl. Mech.*, 2004, **74**, 248–261.

24. Ricoeur, A. and Kuna, M., Influence of electric fields on the fracture of ferroelectric ceramics. *J. Eur. Ceram. Soc.*, 2003, **23**, 1313–1328.
25. Heyer, V., Schneider, G. A., Balke, H., Drescher, J. and Bahr, H.-A., A fracture criterion for conducting cracks in homogeneously poled piezoelectric PZT–PIC151 ceramics. *Acta Mater.*, 1998, **46**, 6615–6622.
26. Hao, T. H. and Shen, Z. Y., A new electric boundary condition of electric fracture mechanics and its applications. *Eng. Fract. Mech.*, 1994, **47**, 793–802.
27. Schneider, G. A., Felten, F. and McMeeking, R. M., The electrical potential difference across cracks in PZT measured by Kelvin Probe Microscopy and the implications for fracture. *Acta Mater.*, 2003, **51**, 2235–2241.
28. Wippler, K., Ricoeur, A. and Kuna, M., Towards the computation of electrically permeable cracks in piezoelectrics. *Eng. Fract. Mech.*, 2004, **71**, 2567–2587.
29. Kemmer, G. and Balke, H., Kraftwirkung auf die Flanken nichtleitender Risse in Piezoelektrika. *GAMM98, short communications in mathematics and mechanics, (ZAMM), Vol. 79 S2*, 1999. p. 509–10.